Edge states and enhanced spin-orbit interaction at graphene/graphane interfaces

Manuel J. Schmidt and Daniel Loss
Department of Physics, University of Basel, Klingelbergstrasse 82, 4056 Basel, Switzerland
(Received 17 March 2010; published 28 April 2010)

We study the electronic properties of interfaces between graphene and graphane, a hydrogenated version of graphene. It is shown that these interfaces are useful for creating an effective edge for the π-electrons of graphene. If the interface is oriented along a zigzag direction, edge states are found. We consider two different interface types, corresponding to usual zigzag and bearded graphene edges. It is shown that, because of a broken symmetry, the spin-orbit interaction is strongly amplified by the graphene/graphane interface and that the edge states are particularly susceptible to this amplification. As an application, we propose a device which is capable of converting spin polarizations to valley polarizations and vice versa. Exploiting the amplification of the spin-orbit interaction, this conversion may be performed at temperatures near one Kelvin. We show that these edge states give rise to quantum spin and/or valley Hall effects.

DOI: 10.1103/PhysRevB.81.165439 PACS number(s): 73.43.−f, 71.70.Ej, 73.63.−b

I. INTRODUCTION

Two-dimensional electronic systems in which the important physics is taking place solely at the edges have received considerable interest during the last decades, starting with the discovery of the quantum Hall effect.[1] In a strong magnetic field, gapless transport channels exist only at the edges of the system and these give rise to a remarkably well-quantized conductance. For a long time, the quantum Hall effect was the only known phase of this type. Recently, however, gapless modes have also been predicted on the surface of topological insulators.[2–4] In contrast to the quantum Hall system, no magnetic field is needed for the generation of edge states in topological insulators. Instead, the spin-orbit interaction (SOI) plays the role of the magnetic field in that it opens a bulk energy gap. The first system in which these states have been investigated is graphene.[2,5,6] It turned out, however, that the SOI in graphene is rather weak.[7] Furthermore, it is difficult to actually construct clean structural edges of graphene, although some experimental progress has been reported.[8]

Recently, a new possibility for the construction of very clean graphene terminations has been proposed:[9,10] rather than structurally cutting graphene in order to create nanostructures, it has been proposed to hydrogenate it locally. Thereby, the π-band is removed wherever graphene is transformed into graphane[11,12] and an *effective edge* is created for the π-electrons. By this technique of local hydrogenation, not only ribbons with high-quality edges of the usual zigzag type (we call them α-edges, henceforth) are possible; also bearded edges (β-edges) are within reach (see Fig. 1).

We study such graphene/graphane (GG) interfaces of α- and β-type and find edge states, which are exponentially localized at the interface. However, instead of being energetically nearly flat, such as in the case of structural graphene edges, the edge states at GG interfaces have a considerable dispersion, the amplitude of which is largely determined by the energy of the hydrogen $1s$-orbital. These edge states enable a quantum spin-valley Hall effect (QSVHE). Moreover, the SOI of these edge states is strongly enhanced due to the proximity of graphane. As an application we propose a device which is capable of converting valley polarizations into spin polarizations and vice versa.

II. EDGE STATES

Henceforth, we assume that all edges and interfaces are oriented along a zigzag direction. Due to the two-atomic unit cell of a hexagonal lattice, there are in principle two different types of boundary conditions—α-type and β-type (see Fig. 1). The reason why a β-edge is seldom considered is that it is highly unstable against structural recombinations.[13] Indeed, we are not aware of any experimental observation of a stable β-edge in graphene.[14] However, if we do not require the graphene flake to be cut in order to generate a β-edge, but only require the hydrogen deposition on graphene to start on a certain sublattice while the hexagonal structure remains intact, it makes not much of a difference whether α- or β-interfaces are to be created.

Before we turn to a more elaborate modeling of GG interfaces and the related edge states which respects the π-band and the σ-band, we would like to start with a qualitative discussion on the basis of a very simplified model which, as it turns out, captures most of the important concepts. We begin with a tight-binding model for the π-electrons in graphene $H_G=t\Sigma_{\langle \mathbf{r},\mathbf{r}'\rangle}c^\dagger_{\mathbf{r}}c_{\mathbf{r}'}$ where $t\simeq -3$ eV, $\langle \mathbf{r},\mathbf{r}'\rangle$ runs over nearest neighbors of a hexagonal lattice $\mathbf{r}=n_1\mathbf{a}_1+n_2\mathbf{a}_2+s\mathbf{R}_1$ ($n_1,\ n_2\in\mathbb{Z},\ s=0,1$) with $\mathbf{a}_1,\mathbf{a}_2$ the Bravais lattice vectors and $\mathbf{R}_1$ the vector connecting the A and B sublattices (see also Fig. 5). $c_{\mathbf{r}}$ is a π-electron annihilation operator. We want to describe geometries which are lattice translationally invariant along a zigzag direction, which we choose to be parallel to $\mathbf{a}_1$ (henceforth, we call this direction the x direction). Thus, it is convenient to transform to electron operators $d_{n,k,s}=N_x^{-1/2}\Sigma_{n_1}e^{-ikn_1}c_{n_1,n,s}$, where N_x is the number of unit cells in the ribbon along the x-direction, so that the one-dimensional (1D) Brillouin zone is $[0,2\pi]$. In terms of the d-operators, the Hamiltonian reads

$$H_G=t\sum_{k,n} d^\dagger_{n,k,A}d_{n,k,B}+d^\dagger_{n,k,A}u_k d_{n-1,k,B}+\text{H.c.}, \qquad (1)$$

where n labels the position along the $\mathbf{a}_2$ direction and $u_k=1+e^{ik}$.

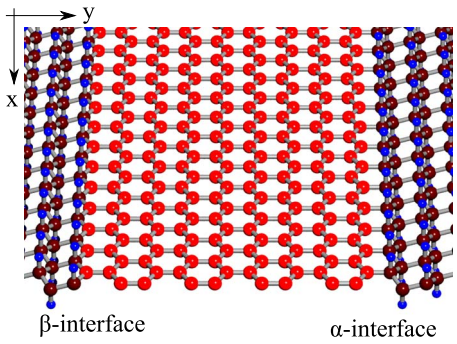

FIG. 1. (Color online) α- and β-interfaces in a graphene/graphane heterostructure. The large (red) spheres represent the carbon atoms and the small (blue) spheres the hydrogen atoms. The brighter spheres correspond to the graphene region while the darker spheres correspond to graphane.

Before we model GG interfaces, we start with a short discussion of the usual structural edges. These edges are obtained from the interface structure, shown in Fig. 1, by completely removing the graphane regions. Later, the GG interfaces are modeled by successively reintroducing terms in the Hamiltonian, which describe hopping between the outermost row of the graphene carbon atoms and the carbon atoms in the graphane region.

In the Hamiltonian (1), a structural α-edge is introduced by removing all terms with operators corresponding to positions $n<0$ and the terms with operators corresponding to the A sublattice site of $n=0$. For a β-edge only the $n<0$ terms need to be removed (see Appendix A). A Hamiltonian truncated in such a way gives rise to exponentially localized, edge states with zero energy[15]

$$|\psi_0^{\alpha/\beta}(k)\rangle = \mathcal{N}_k^{\alpha/\beta}\sum_{n=0}^{\infty} e^{-n/\xi_k^{\alpha/\beta}+in\phi} d_{n,k,B/A}^\dagger|0\rangle, \tag{2}$$

with the normalization constant $\mathcal{N}_k^{\alpha,\beta}=(1-|u_k|^{\pm 2})^{1/2}$, the localization length $\xi_k^{\alpha,\beta}=\mp[\ln|u_k|]^{-1}$ and some unimportant phase $\phi=\arg(-u_k^{\pm 1})$. Obviously, the α-edge state only exists for $k\in(\frac{2\pi}{3},\frac{4\pi}{3})$ while the remaining k-space supports the β-edge state. At the projections of the valleys K and K' to the 1D Brillouin zone, i.e., $K\to\frac{2\pi}{3}$ and $K'\to\frac{4\pi}{3}$, the localization lengths of both edge states diverge as $\frac{2}{\sqrt{3}}|k-K|^{-1}$ or $\frac{2}{\sqrt{3}}|k-K'|^{-1}$, respectively.

For a ribbon with α- and β-edges on opposite sides, a zero energy mode is present throughout the whole Brillouin zone. For $k\in(\frac{2\pi}{3},\frac{4\pi}{3})$, the wave function of this mode is exponentially localized at the α-edge, whereas for $k\in(-\frac{2\pi}{3},\frac{2\pi}{3})$ it is localized at the β-edge. Directly at K or K', the wave function of the zero energy mode is completely delocalized over the ribbon.

Now, instead of a structural graphene edge we want to describe a GG interface (we discuss only the α-interface, the β-interface being analogous; see also Appendix A). The essential features are well described within a simplified model which includes only one -C-H group at each "tooth" of the zigzag edge (see also Fig. 5), instead of the whole graphane lattice. We further neglect all σ-orbitals of the carbon atoms. The Hamiltonian of this -C-H group reads

$$H_I = td_{k,C}^\dagger d_{0,k,B} + t' d_{k,H}^\dagger d_{k,C} + \text{H.c.} + \epsilon_H d_{k,H}^\dagger d_{k,H}, \tag{3}$$

and must be added to the α-truncated H_G, where $d_{k,C}$ and $d_{k,H}$ are the annihilation operators of the carbon π-orbital and the hydrogen s-orbital, respectively. Typically, $\epsilon_H\simeq -0.4$ eV is much smaller than the other two energy scales $t\simeq -3$ eV and $t'\simeq -5.8$ eV (see Appendix B). Since we are only interested in how the -C-H group affects the edge state [Eq. (2)], we project H_G+H_I onto the subspace spanned by the edge state and the relevant additional atomic orbitals on the C atom ($2p_z$-orbital) and the H atom ($1s$-orbital), i.e., $\{|\psi_0^\alpha(k)\rangle, |C\rangle=d_{k,C}^\dagger|0\rangle, |H\rangle=d_{k,H}^\dagger|0\rangle\}$. The operators $d_{k,H}$ and $d_{k,C}$ are defined in analogy to the operators $d_{n,k,s}$. The neglect of the $2s$-, $2p_x$-, and $2p_y$-orbitals on the additional carbon atom is justified because the edge state is decoupled from them by symmetry. The neglect of the other bulk states of the graphene is justified by their higher energy and the small weight of their wave functions at the outermost row of atoms. Below, we further justify the use of this model by a comparison with an extended tight-binding calculation. The projected Hamiltonian reads

$$H_{\text{proj.}} = \begin{pmatrix} 0 & t\mathcal{N}_k^\alpha & 0 \\ t\mathcal{N}_k^\alpha & 0 & t' \\ 0 & t' & \epsilon_H \end{pmatrix}. \tag{4}$$

In leading order perturbation theory in $\frac{\epsilon_H}{t'}$ and $\frac{t}{t'}$, this projection yields a low-energy edge state $|\psi^\alpha(k)\rangle\propto t'|\psi_0^\alpha(k)\rangle - t\mathcal{N}_k^\alpha|H\rangle+\mathcal{O}(\epsilon_H)|C\rangle$ with energy

$$\epsilon^\alpha(k) \simeq \epsilon_H\frac{t^2}{t'^2}[2\cos(k-\pi)-1], \quad k\in\left[\frac{2\pi}{3},\frac{4\pi}{3}\right], \tag{5}$$

where we have dropped terms of order $\frac{\epsilon_H^2}{t'^2}$ and $\frac{t^4}{t'^4}$. Note that the amplitude of the state $|\psi^\alpha(k)\rangle$ is of order ϵ_H at the C atom of the -C-H group. As a result, the inclusion of more and more graphane rows, i.e., -C-H groups, only leads to terms of higher order in ϵ_H/t'. Thus, this simplified model is expected to describe the energy dispersion correctly as long as no other states which we have neglected here come too close in energy. Equation (5) roughly describes a parabola around $k=\pi$ which crosses zero at K and K'. The edge state at a GG interface has—in contrast to the edge state at a structural zigzag edge—a finite velocity, the magnitude of which is largely determined by the energy of the hydrogen $1s$-orbital ϵ_H relative to the π-orbital energy in graphene (set to zero here). Note that also other effects which are not included in our simplified model, e.g., next-nearest-neighbor hoppings[16] or local electrostatic gates at the edges,[17] can increase the bandwidth of the edge state. For typical parameters we obtain edge state velocities of 10^4-10^5 m/s (see Appendix A).

The bandwidth of the edge state is crucial for the question of magnetic ordering at the edges. Conventional graphene edges are believed to be spin-polarized in their ground state,[18,19] because the electron-electron interactions are much larger than the bandwidth of the edge state. An instability, very reminiscent of a Stoner instability, then leads to a po-

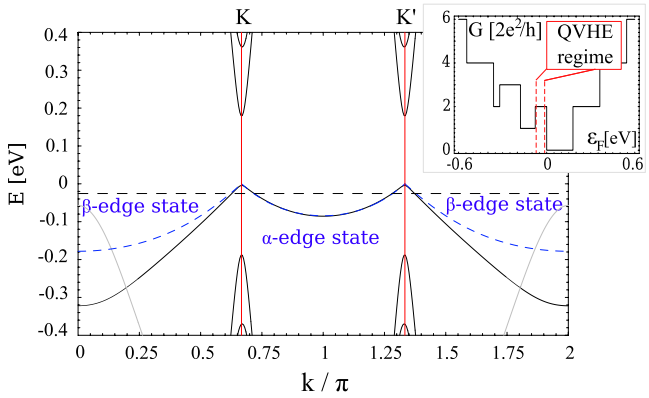

FIG. 2. (Color online) The band structure of a graphane-terminated $\alpha\beta$-ribbon with $W=10$ nm. The dashed horizontal line is a typical Fermi energy ϵ_F for the QVHE regime chosen such that $\xi_{k_F} \ll W/2$. The gray bands correspond to exponentially localized states at the outer graphane edge, which are not important here. The full curves are results of numerical calculations within the extended tight-binding model. The dashed (blue) curves show the effective model dispersion [Eq. (5)]. The inset shows the conductance G of the graphene region as a function of ϵ_F.

larized ground state. In addition to this, Lieb's theorem[20] suggests that the ground state should be spin-polarized at a zigzag edge, where there is a local imbalance between the number of A and B sublattice sites. However, Lieb's theorem is only applicable in particle-hole symmetric systems. The graphane termination breaks this symmetry so that Lieb's theorem is not applicable any longer. However, the question is: is this symmetry breaking strong enough to drive the edge out of the ferromagnetic phase. To answer this, one must compare the strength of the electron-electron interactions with the bandwidth of the edge state. A large bandwidth corresponds to a strong breaking of the electron-hole symmetry and thus favors a non-magnetic ground state. Experimentally, the bandwidth can be tuned further by electrostatic gates so that one should be able to depolarize the edge at GG interfaces.[17,21]

Figure 2 compares the energy dispersion of the edge states calculated from the extended tight-binding model, as introduced below, with Eq. (5) and its analog for the β-edge state (see Appendix A). While the simplified model for the α-edge state agrees well with the extended model, the simplified β-edge state dispersion predicts a too small bandwidth. However, the main features, namely the different directions of motion of electrons in the valley K (K') at different interfaces, are described properly by the simplified model.

III. EDGE STATE TRANSPORT

A ribbon with combined α- and β-interfaces ($\alpha\beta$-ribbon) with finite width W of the graphene region gives rise to a quantum valley Hall effect (QVHE),[22] in which K (K') valley electrons move left (right) at the α-interface and right (left) at the β-interface, if the Fermi energy ϵ_F is tuned as indicated in Fig. 2. For wide enough ribbons ($\xi_{k_F} \ll W/2$), the overlap between edge states moving in different directions is small so that backscattering is forbidden if valley scattering can be neglected. Since valley scattering requires the transfer of a large crystal momentum, only atomic scale disorder would destroy the QVHE.

The detection of this QVHE by a transport measurement could be a first experimental step to reveal the GG interface quality. In a clean $\alpha\beta$-ribbon the conductance is $\frac{2e^2}{h}n$, where n is the number of transport modes intersected by ϵ_F (see inset of Fig. 2). Disorder on the scale of the lattice constant, however, induces valley scattering and the backscattering processes at a single edge become important. This is similar to introducing magnetic impurities at the edge of a QSHE system.

For wide ($W \gg 50$ nm)$\alpha\beta$-ribbons at temperatures below the spin-orbit gap in bulk graphene [~ 10 mK (Ref. 7)] a new quantized Hall effect arises: the QSVHE. Here, not only the spin or the valley determines the direction of motion at the edges, like in the QSHE[2] or in the QVHE, respectively, but both, *spin and valley* are responsible for the selection of the edge and the direction of motion, if ϵ_F is tuned into the bulk SOI-induced gap in graphene. For instance, at an α-interface only electrons in valley K and with spin pointing into a certain direction (we define this direction as $\uparrow$) are allowed to move left; the electron in valley K' and with spin pointing into the opposite direction ($\downarrow$) moves right. The other two combinations of valley and spin are not allowed. This increases the stability of the QSVHE compared to the pure QSHE or QVHE because backscattering requires simultaneous valley and spin scattering. In principle the QSVHE already allows spin-valley conversion, but only at very low temperatures (~ 10 mK). In the next section we show how GG interfaces may be used to perform spin-valley conversion at much higher temperatures.

IV. ENHANCED SPIN-ORBIT INTERACTION

It is well known that the smallness of the SOI in graphene is rooted in the lightness of carbon on one hand and in the symmetry-induced decoupling of the π- and σ-bands, on the other. The latter issue can be overcome, however, by breaking the $\pm z$ symmetry of the lattice. While the carbon atoms of the A and B sublattices are coplanar in graphene, they are "pushed" out of the plane in graphane due to the rehybridization $sp_2 \rightarrow sp_3$ which is caused by the presence of the additional hydrogen atoms.[11] As a result, the hopping between π-band orbitals and σ-band orbitals on neighboring carbon sites is allowed in graphane and at the GG interface, so that the π-band is locally coupled to the σ-band at the interface. Note that, in addition to this direct hopping, also a strong indirect coupling between the carbon π- and σ-orbitals via the hydrogen atom takes place in graphane. This indirect coupling is independent of the details of the interface geometry. For these reasons, we expect an enhanced SOI near GG interfaces.

In order to substantiate this expectation, we use an extended tight-binding model for GG heterostructures, which respects the π- as well as the σ-orbitals of the carbon atoms. It is based on an environment-dependent tight-binding model for general hydrocarbons[23,24] and takes the atomic carbon

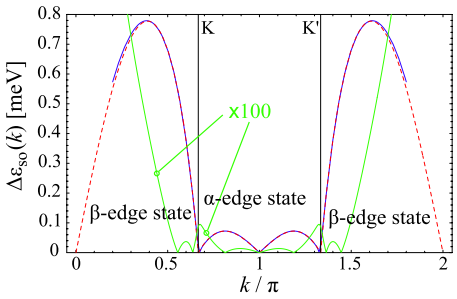

FIG. 3. (Color online) SOI-induced spin-splitting of the edge states. The solid black (blue) curve shows the absolute value of the spin-splitting $\Delta\epsilon_{SO}(k)$ of the edge states calculated from the extended tight-binding model with the full SOI. This calculation has been done for a 10 nm wide $\alpha\beta$-ribbon. The dashed (red) line shows the spin-splitting calculated from the effective Hamiltonian (9). The spin-splitting at K,K' which is slightly larger than the spin-orbit splitting in bulk graphene is due to finite-size effects. The gray (green) curve shows the spin-orbit splitting of the edge states without graphene termination, scaled up by a factor of 100. This calculation has also been done within the extended tight-binding model (without the graphane regions), as described in Appendix C.

SOI into account.[7] More information about the extended tight-binding model can be found in the Appendix B. For simplicity, we discuss interfaces in which the first row of the graphane lattice is coplanar with the graphene region. Note, however, that our results also apply to tilted interfaces, as discussed in detail in the Appendices E and F. We find that the GG edge states exhibit a much larger spin-splitting than conventional edge states. Figure 3 compares the spin-splitting of the edge states of a graphane-terminated $\alpha\beta$-ribbon with the situation in a usual $\alpha\beta$-nanoribbon without graphene termination. This can be understood for the α-edge state by projecting the on-site SOI Hamiltonian

$$H_{SO} = i\Delta \sum_{\mathbf{r}} \sum_{\mu\nu\rho\tau\tau'} \epsilon^{\mu\nu\rho} c^{\dagger}_{\mathbf{r},p_\mu,\tau} \sigma^{\nu}_{\tau\tau'} c_{\mathbf{r},p_\rho,\tau'}, \tag{6}$$

where $c_{\mathbf{r},p_\mu,\tau}$ annihilates an electron at site $\mathbf{r}$ in orbital p_μ with spin τ, σ^μ are the Pauli matrices for the electron spin, $\mu,\nu,\rho = x,y,z$, $\Delta \simeq 3$ meV is the strength of the atomic SOI of carbon,[7] and $\epsilon^{\mu\nu\rho}$ is the Levi-Civita tensor, onto the two-dimensional spin-degenerate subspace of the α-edge state $|\psi^\alpha(k);\tau\rangle$ obtained by diagonalizing the extended tight-binding Hamiltonian without SOI. In a conventional edge state $|\psi_0^\alpha(k);\tau\rangle$ (without graphane termination) only the π-orbitals are occupied so that $\langle\psi_0^\alpha(k);\tau|H_{SO}|\psi_0^\alpha(k);\tau'\rangle \equiv 0$ and the SOI becomes a second order effect.[7] At a GG interface, however, the edge state acquires contributions from the σ-orbitals because of the $\pm z$ symmetry breaking which leads to a mixing of the π- and the σ-band. As a result, the SOI becomes a first order effect. Since the energy scale of the hopping Hamiltonian is a few eV while the energy scale of the SOI Hamiltonian is a few meV, this leads to an amplification of SOI effects by a factor of 10^2–10^3. This is the fundamental reason for the enhancement of SOI effects at GG interfaces, as compared to pure graphene nanoribbons.

The projected SOI Hamiltonian for the α-edge state reads

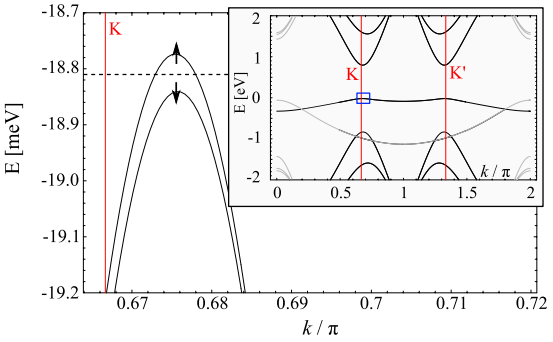

FIG. 4. (Color online) Energy dispersion of the edge states of a 2 nm wide $\alpha\beta$-ribbon near the K-valley. The two bands have opposite spin direction. The dashed line indicates a typical ϵ_F. The inset shows a larger region of the band structure. The gray lines are bulk graphane states and states at the outer graphane edge which are not of interest here.

$$H_{SO}^{\mathrm{eff},\alpha} = \sum_{\tau\tau'} \int_{2\pi/3}^{4\pi/3} \frac{dk}{2\pi} e^{\dagger}_{k,\alpha,\tau} \Gamma_{\tau\tau'}(k) e_{k,\alpha,\tau'}, \tag{7}$$

with $e_{k,\alpha,\tau}$ the α-edge state annihilation operators and

$$\Gamma_{\tau\tau'}(k) = \langle\psi^\alpha(k);\tau|H_{SO}|\psi^\alpha(k);\tau'\rangle, \tag{8}$$

$$\simeq (k-\pi)(\mathcal{N}_k^\alpha)^2[\Delta_R^\alpha \sigma^y + \Delta_i^\alpha \sigma^z]_{\tau\tau'}, \tag{9}$$

where Δ_R, Δ_i are constants describing the Rashba and intrinsic parts of the effective SOI, respectively. The Dresselhaus term ($\propto\sigma^x$) vanishes because of the mirror symmetry $x \to -x$ of the interfaces. The additional factor $(\mathcal{N}_k^\alpha)^2$ accounts for the fact that the effective SOI, generated by a GG interface, must be proportional to the weight of the edge state wave function at the interface. The parameters $\Delta_R^\alpha = -0.09$ meV and $\Delta_i^\alpha = 0.021$ meV are obtained from a fit to the numerical results (for details see Appendix F). Because of time-reversal invariance the spin-splitting is exactly zero at $k = 0, \pm\pi$. These are also the points where the spin direction of the energetically higher edge state changes abruptly. Note that for wide ribbons ($W \gtrsim 100$ nm), the spin-splitting at K,K' is essentially given by the bulk SOI of graphene because $\mathcal{N}_k^{\alpha/\beta}$ vanishes for $k \to K,K'$. As a result, the SOI enhancement at the interfaces does not increase the critical temperature at which the QSVHE can be observed.

However, there is another possibility to use the interfacial enhancement of the SOI for high-temperature spin-valley conversion. Because the SOI enhancement is proportional to the weight of the edge state wave functions at the interface, it is obvious that the enhancement of the edge states' spin-splitting at K and K' decays as W^{-1} (see also Appendix F). In the limit of wide ribbons the (very small) spin-orbit splitting of bulk graphene is approached. This is because at K and K', due to the complete delocalization of the edge state, the weight of the edge state wave function at the interface is vanishingly small, and so is the SOI enhancement from the interface. Thus, one should use narrow ribbons in order to exploit the SOI enhancement at GG interfaces. In Fig. 4, the band structure of a narrow GG heterostructure is shown. At

the maxima of the edge mode the spin-orbit splitting is about 0.07 meV$\simeq$0.8 K. Note that although these states are derived from edge states, they do not actually appear like edge states in this case because $\xi_k \gg W$ (ξ_k diverges near K and K'). Thus, by squeezing the wide edge states into a narrow ribbon, the spin-orbit splitting is enhanced at K and K'. Even narrower ribbons exhibit even larger spin-orbit splittings.

As required, the energetically higher band at K has the opposite spin-direction than the corresponding band at K'. Thus, by tuning ϵ_F as indicated in Fig. 4, a spin-valley filter is realized: left- and right-movers exist for each spin and valley but the transmission of this structure is only non-zero for $(K,\uparrow)$ or for $(K',\downarrow)$ and zero for the other two combinations of valley and spin. This means that each spin-up electron which initially consists of K and K' components (valley-unpolarized) will be in a pure valley state (K here) after it has passed the narrow $\alpha\beta$-ribbon in x-direction, while a valley-unpolarized spin-down electron will be in a pure K' state after the passage. This filtering works also in the opposite way, i.e., a valley polarization results in spin polarization after passage.

V. CONCLUSION

We have demonstrated that a termination of graphene nanoribbons by graphane can be utilized to create an effective edge for the π-band in graphene. This effective edge features edge states, similar to the usual zigzag edge states that are well known in zigzag nanoribbons of pure graphene. In addition to this, two advantageous properties of graphene/graphane interfaces are found: (a) the bandwidth of the edge states at graphene/graphane interfaces is enhanced compared to the bandwidth of edge states at usual graphene edges. The bandwidth enhancement is proportional to the energy of the hydrogen 1s-orbital. This suggests tuning the bandwidth by electrostatic gates or by alternative adsorbates with a different orbital energy than hydrogen. (b) due to the $\pm z$ symmetry breaking in graphane, a strongly enhanced spin-orbit interaction exists at the interface which affects foremost the edge states.

These additional features may be exploited in the construction of nanoribbons with special properties. The larger bandwidth of the edge states and its tunability may be used to drive the edges out of their spin-polarized phase.[21] We have shown that a narrow nanoribbon in the spin-unpolarized phase can be used as a device that converts spin polarization into valley polarization and vice versa. Due to the enhanced spin-orbit interaction at the interface, the operation temperature of this device may well be near one Kelvin.

It should also be noted that graphene/graphane interfaces provide a means to construct (effective) bearded edges. In usual graphene nanoribbons, these would be very unstable. Very recently, the stability of graphene/graphane interfaces has been studied in Refs. 25 and 26. They found that very narrow graphane-terminated graphene nanoribbons are stable and even that there is a tendency to atomically sharp interfaces. These papers suggest that it might indeed be possible to make rugged graphene/graphane interfaces atomically sharp by annealing, e.g., with protocols similar to the one used in Ref. 8.

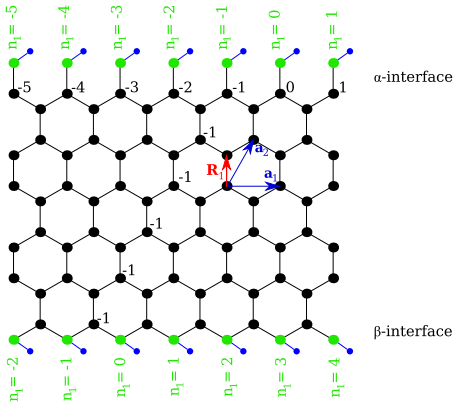

FIG. 5. (Color online) Definitions in the simplified interface model. The gray (green) dots represent the carbon atoms of the -C-H groups and the small black (blue) dots represent the hydrogen atoms. The number labels indicate the n_1 coordinate of the carbon atoms in the graphene region.

ACKNOWLEDGMENTS

We acknowledge useful discussions with B. Braunecker, I. Martin, B. Trauzettel, and A. Yacoby. We also thank R. Grassi for helpful remarks. This work has been supported by the Swiss NF and the NCCR Nanoscience Basel.

APPENDIX A: SIMPLIFIED MODEL FOR THE EDGE STATE

The α- and β-truncated Hamiltonians for the structural graphene zigzag edges read

$$H_G^{\alpha} = t\sum_k \sum_{n=1}^{\infty} [d_{n,k,A}^{\dagger} d_{n,k,B} + d_{n,k,A}^{\dagger} u_k d_{n-1,k,B}], \tag{A1}$$

$$H_G^{\beta} = t\sum_k \left\{ \sum_{n=1}^{\infty} [d_{n,k,A}^{\dagger} d_{n,k,B} + d_{n,k,A}^{\dagger} u_k d_{n-1,k,B}] + d_{0,k,A}^{\dagger} d_{0,k,B} \right\}, \tag{A2}$$

with $u_k = 1 + e^{ik}$ and the simplified model Hamiltonians for the α- and β-interfaces between graphene and graphane read

$$H_I^{\alpha} = t d_{k,C}^{\dagger} d_{0,k,B} + t' d_{k,H}^{\dagger} d_{k,C} + \text{H.c.} + \epsilon_H d_{k,H}^{\dagger} d_{k,H} \tag{A3}$$

$$H_I^{\beta} = t u_k d_{k,C}^{\dagger} d_{0,k,B} + t' d_{k,H}^{\dagger} d_{k,C} + \text{H.c.} + \epsilon_H d_{k,H}^{\dagger} d_{k,H}, \tag{A4}$$

where we have defined

$$d_{k,H} = N_x^{-1/2} \sum_{n_1} e^{-ikn_1} c_{n_1,H} \tag{A5}$$

$$d_{k,C} = N_x^{-1/2} \sum_{n_1} e^{-ikn_1} c_{n_1,C}. \tag{A6}$$

The operators $c_{n_1,C}$ annihilate an electron in the π-orbital of the carbon atom next to the edge, as shown in Fig. 5 and the operators $c_{n_1,H}$ annihilate an electron in the 1s-orbital of the corresponding hydrogen atom.

The projection of $H_G^{\alpha/\beta}+H_I^{\alpha/\beta}$ onto the subspaces $\{|\psi_0^{\alpha/\beta}(k)\rangle,\ |C\rangle=d_{k,C}^\dagger|0\rangle,\ |H\rangle=d_{k,H}^\dagger|0\rangle\}$ reads in matrix form

$$[H_G^\alpha+H_I^\alpha]_{\text{proj.}}=\begin{bmatrix}0 & t\mathcal{N}_k^\alpha & 0\\ t\mathcal{N}_k^\alpha & 0 & t'\\ 0 & t' & \epsilon_H\end{bmatrix}, \tag{A7}$$

$$[H_G^\beta+H_I^\beta]_{\text{proj.}}=\begin{bmatrix}0 & tu_k\mathcal{N}_k^\beta & 0\\ tu_k^*\mathcal{N}_k^\beta & 0 & t'\\ 0 & t' & \epsilon_H\end{bmatrix}. \tag{A8}$$

Because $|\epsilon_H|\ll|t|,|t'|$, we are only interested in results to leading order in ϵ_H. We find a low-energy edge state for both α- and β-interfaces

$$\epsilon^\alpha=\frac{t^2(\mathcal{N}_k^\alpha)^2}{t^2(\mathcal{N}_k^\alpha)^2+t'^2}\epsilon_H+\mathcal{O}(\epsilon_H^2),\quad k\in\left[\frac{2\pi}{3},\frac{4\pi}{3}\right], \tag{A9}$$

$$\epsilon^\beta=\frac{t^2|u_k|^2(\mathcal{N}_k^\beta)^2}{t^2|u_k|^2(\mathcal{N}_k^\beta)^2+t'^2}\epsilon_H+\mathcal{O}(\epsilon_H^2),\quad k\in\left[-\frac{2\pi}{3},\frac{2\pi}{3}\right]. \tag{A10}$$

Near the boundary of the k-space domains of the edge states, $K=\frac{2\pi}{3}$ and $K'=\frac{4\pi}{3}$, the dispersion is approximately linear and we can write for both states (α/β) in both valleys (K,K')

$$\epsilon^{\alpha/\beta}=\sqrt{3}\frac{t^2\epsilon_H}{t'^2}|\delta k|+\mathcal{O}(\delta k^2), \tag{A11}$$

where $\delta k=k-K$ or $\delta k=k-K'$. From this we can estimate the typical velocity of the edge states near K and K' to

$$|v^{\alpha/\beta}|\simeq\sqrt{3}\frac{t^2|\epsilon_H|}{t'^2}\frac{a_0\sqrt{3}}{\hbar}\simeq 10^5\frac{\text{m}}{\text{s}}, \tag{A12}$$

which is about one order of magnitude smaller than the Fermi velocity in graphene.

Next, we would like to estimate the typical localization length of the edge states in the QSVHE regime. If we take the SOI into account, a spin gap $\Delta\simeq 2\ \mu$eV opens up at K and K' for wide ribbons ($W\gtrsim 100$ nm). This spin gap is of the order of the spin-orbit splitting in bulk graphene because the edge states become completely delocalized over the graphene region at K and K'. If the Fermi energy is of the order of the spin gap, the four Fermi momenta can be estimated by

$$k_F^{1/2}\simeq K\pm\Delta\frac{t'^2}{\sqrt{3}t^2\epsilon_H}\simeq K\pm 3.4\cdot 10^{-3}\pi, \tag{A13}$$

$$k_F^{3/4}\simeq K'\pm\Delta\frac{t'^2}{\sqrt{3}t^2\epsilon_H}\simeq K'\pm 3.4\cdot 10^{-3}\pi. \tag{A14}$$

From this, the corresponding localization lengths for all interface states in the QSVHE regime are

$$\xi_{k_F}^{\alpha/\beta}=\frac{3}{2}a_0|\ln|u_{k_F}\|^{-1}\simeq 22\ \text{nm}, \tag{A15}$$

with $a_0\simeq 1.4$ Å the nearest-neighbor C-C distance.

TABLE I. Two sets of nearest-neighbor tight-binding parameters from the literature. In the following, we use the second column of parameters.

	Reference 24 (eV)	Reference 27 (used here) (eV)
V_{ss}	−4.6	−6.8
V_{pp}^π	−2.4	−3.0
V_{pp}^σ	−6.5	−5.0
V_{sp}	−4.7	−5.6

APPENDIX B: TIGHT-BINDING PARAMETERS

We want to model the graphene/graphane heterostructures by a nearest-neighbor tight-binding model which takes into account the π-band and the σ-band of the hexagonal carbon backbone and the $1s$-orbitals of the hydrogen atoms attached to each C atom in the graphane region. We neglect the nonorthogonalities of orbitals on different sites. First of all, we need the bare tight-binding hopping integrals between the oriented carbon orbitals $2s$, $2p_x$, $2p_y$, $2p_z$, i.e., the matrix elements of the Hamiltonian H

$$V_{ss}=\langle 2s;\mathbf{r}_0|H|2s;\mathbf{r}_1\rangle, \tag{B1}$$

$$V_{sp}=\langle 2p_z;\mathbf{r}_0|H|2s;\mathbf{r}_1\rangle, \tag{B2}$$

$$V_{pp}^\sigma=-\langle 2p_z;\mathbf{r}_0|H|2p_z;\mathbf{r}_1\rangle, \tag{B3}$$

$$V_{pp}^\pi=\langle 2p_x;\mathbf{r}_0|H|2p_x;\mathbf{r}_1\rangle, \tag{B4}$$

and the hopping integrals between carbon orbitals and the hydrogen $1s$-orbital

$$W_{ss}=\langle 1s;\mathbf{r}_0|H|2s;\mathbf{r}_2\rangle, \tag{B5}$$

$$W_{sp}=\langle 2p_z;\mathbf{r}_0|H|1s;\mathbf{r}_2\rangle, \tag{B6}$$

where $\mathbf{r}_0=(0,0,0)^T$, $\mathbf{r}_1=a_0(0,0,1)^T$, and $\mathbf{r}_2=b_0(0,0,1)^T$ with a_0 the nearest-neighbor C-C distance and b_0 the C-H distance. The kets $|2s;\mathbf{r}\rangle,|2p_i;\mathbf{r}\rangle$ represent the $2s$- and the $2p_i$-orbitals $(i=x,y,z)$ of the carbon atoms at $\mathbf{r}$. The ket $|1s;\mathbf{r}\rangle$ represents the hydrogen $1s$-orbital.

The H-H distance in the chair conformation of graphane is large enough so that the direct hopping between hydrogen orbitals may be neglected. All nearest-neighbor hopping integrals between the relevant orbitals in graphane can be reduced to the parameters defined in Eqs. (B1)–(B6), as we will show subsequently.

In general, these bare hopping parameters are environment-dependent.[23,24] However, there is a considerable variance of hopping parameters in the literature. For instance, the very often used parameters in Ref. 27 deviate considerably from the ones extracted from Ref. 24 (see Table I). In this case, the deviation is probably due to the different scopes of Refs. 24 and 27, namely, the crystal structure and the electronic properties, respectively. Therefore, we believe that the carbon orbital hopping parameters of Ref. 27 are more suitable to our needs. Furthermore, as Reich *et al.*

argue[28] for the π-band, for a quantitative description one would have to include up to 3rd neighbor hoppings and the corresponding non-orthogonalities. These parameters are, however, to our best knowledge, not available for the σ-band in graphene. Since we only aim at a description on a qualitative level, we refrain from a more quantitative first principles calculation. We rather check that our results are robust with respect to variations in the parameters.

Furthermore, we make the simplifying assumption that the bare hopping matrix elements are the same in the graphene and in the graphane region. This does not mean, of course, that the final Hamiltonian in the carbon subspace is equal for graphene and graphane. The different relative alignment of the A- and the B-sublattice is taken into account later.

The parameters for the C-H bond in the graphane region (W_{ss} and W_{sp}) are calculated along the lines of Ref. 23, with a C-H bond length of 1.1 Å.[11] They are

$$W_{ss} = -5.4 \text{ eV}, \quad W_{sp} = -5.8 \text{ eV}. \tag{B7}$$

Finally, the $2p$-orbital energy of carbon defines the zero of the energy. The relative energy of the carbon $2s$-orbital is $\epsilon_C^s = -8.7$ eV.[27] The orbital energy of the hydrogen $1s$-orbital can be roughly estimated from Refs. 23 and 24. We assume that the orbital energies of the carbon orbitals are elevated due to the nearby hydrogen atom about the same amount as due to the other carbon atoms. In this work we use $\epsilon_H^s = -0.4$ eV for the hydrogen $1s$-orbital. The results and conclusions do not depend critically on this value.

APPENDIX C: ORBITAL RIBBON HAMILTONIAN

We first want to derive the Hamiltonian, describing bulk graphane and bulk graphene, in order to check the resulting band structure against *ab initio* band structures in the literature.[11] For doing this, we need to translate the bare hopping integrals Eqs. (B1)–(B7) to the hoppings on the lattice under consideration. We define the honeycomb lattice vectors $\mathbf{a}_1 = a_0(\sqrt{3},0,0)^T$ and $\mathbf{a}_2 = a_0(\frac{\sqrt{3}}{2},\frac{3}{2},0)^T$ and the nearest-neighbor vectors

$$\mathbf{R}_1 = a_0(0,1,z)^T, \tag{C1}$$

$$\mathbf{R}_2 = a_0\left(-\frac{\sqrt{3}}{2},-\frac{1}{2},z\right)^T, \tag{C2}$$

$$\mathbf{R}_3 = a_0\left(\frac{\sqrt{3}}{2},-\frac{1}{2},z\right)^T, \tag{C3}$$

where a_0 is the C-C distance of flat graphene and za_0 is the separation of the A- and B-sublattice planes. We choose the parameter $z = z_0 \simeq 0.42$ in this work. At each carbon site, we define the system of the $2s$- and $2p$-orbitals in the following way: the s-orbital is spherically symmetric, so that the atomic alignment is irrelevant. The p-orbitals can be characterized by a vector, pointing into the direction of the positive part of the orbital wave function. The wave functions of the second carbon shell are approximately

$$\psi_{2s}(\mathbf{r}) = f_{2s}(|\mathbf{r}|), \tag{C4}$$

$$\psi_{2p_i}(\mathbf{r}) = f_{2p}(|\mathbf{r}|)r_i, \quad i = x,y,z. \tag{C5}$$

Thus, we choose the alignment of the three $2p$-orbitals according to the same coordinate system, which defines $\mathbf{a}_1, \mathbf{a}_2$. Note that the p-orbitals transform as a vectors. This is useful if we want to express a p-orbital pointing, say, into the (1,1,0) direction. The wave function of this orbital can be written in terms of the basis functions Eq. (C5),

$$\psi_{2p,(1,1,0)}(\mathbf{r}) = \frac{1}{\sqrt{2}}[\psi_{2p_x}(\mathbf{r}) + \psi_{2p_y}(\mathbf{r})]. \tag{C6}$$

The direction of an orbital is conveniently expressed by a vector $\mathbf{p}$.

We need to deal with three different types of C-C hoppings. There is the hopping from an s-orbital to another s-orbital (ss), the hopping from an s-orbital to a p-orbital (sp) and the hopping between p-orbitals (pp). For the subsequent discussion we introduce the bond vector $\mathbf{r}_b$ which connects the two atoms participating in the bond under consideration. For an sp-bond $\mathbf{r}_b$ points always from the atom, carrying the s-orbital, to the atom on which the p-orbital is located. For ss-bonds and pp-bonds the direction of $\mathbf{r}_b$ plays no role.

The ss-hopping does not depend on the direction of $\mathbf{r}_b$ but only on the bond length. The bond length, however, is assumed constant over the whole lattice. In a homogeneous structure (only graphene or graphane), this assumption is fulfilled perfectly. In a heterostructure such as the one we aim to describe there is a minor difference in the bond lengths in the different regions. We neglect this difference in the bond length because we believe that the dominant difference between graphene and graphane is the different symmetry of the lattice.

For sp-hopping we only know the hopping integral if the p-orbital is aligned along the bond vector. The hopping between an s-orbital and a p-orbital that is perpendicular to the bond vector is zero by symmetry. Thus, only the angle θ between the p-orbital and the bond vector is important (see Fig. 6). The sp-hopping integral of such a bond is then

$$t_{sp}(\theta) = -V_{sp}\cos\theta, \quad \cos\theta = \frac{\mathbf{r}_b \cdot \mathbf{p}}{|\mathbf{r}_b||\mathbf{p}|}. \tag{C7}$$

For pp-hopping, three angles are relevant: the two angles θ_1, θ_2 between the p-orbitals $\mathbf{p}_1, \mathbf{p}_2$ and the bond vector $\mathbf{r}_b$ (see Fig. 6) and the angle ρ between the planes spanned by $\mathbf{r}_b$, $\mathbf{p}_1$ and $\mathbf{r}_b$, $\mathbf{p}_2$. The hopping integral of such a bond is

$$t_{pp}(\theta_1,\theta_2,\rho) = \cos\theta_1 \cos\theta_2 V_{pp}^{\sigma} + \sin\theta_1 \sin\theta_2 \cos\rho V_{pp}^{\pi} \tag{C8}$$

with

$$\cos\theta_1 = -\frac{\mathbf{r}_b \cdot \mathbf{p}_1}{|\mathbf{r}_b||\mathbf{p}_1|}, \quad \cos\theta_2 = \frac{\mathbf{r}_b \cdot \mathbf{p}_2}{|\mathbf{r}_b||\mathbf{p}_2|}, \tag{C9}$$

and

$$\rho = \sphericalangle[\mathbf{r}_b \times \mathbf{p}_1, \mathbf{r}_b \times \mathbf{p}_2]. \tag{C10}$$

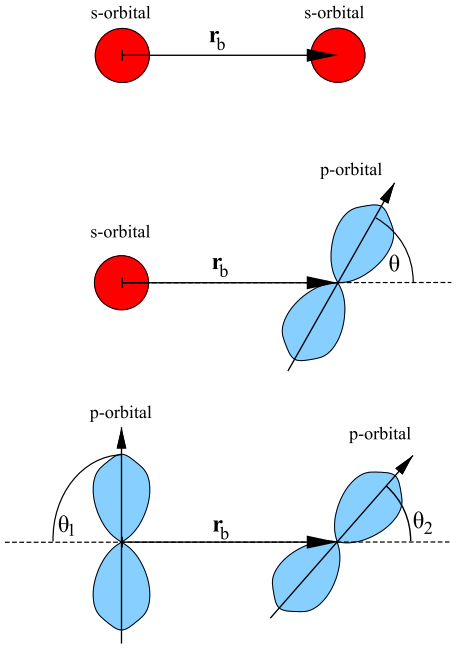

FIG. 6. (Color online) Relative orientation of the carbon s- and p-orbitals. $\mathbf{r}_b$ is the bond vector, connecting the positions of the two atoms.

With the above equations we can evaluate all hopping matrix elements we need to write down the Hamiltonian. We start with the Hamiltonian in the carbon subspace H_C. We denote the sublattice by $s=A,B$, the Bravais lattice vector $\mathbf{R_n}=n_1\mathbf{a}_1+n_2\mathbf{a}_2$ and the orbitals by $\mu=0,1,2,3$ for the s-, p_x-, p_y-, and p_z-orbital, respectively. The real-space Hamiltonian reads

$$H_C = \sum_{\mathbf{n},\mu,\mu'} c^\dagger_{\mathbf{n},\mu,A}[t_{\mu,\mu',1}c_{\mathbf{n},\mu',B} + t_{\mu,\mu',2}c_{\mathbf{n}-(0,1),\mu',B} + t_{\mu,\mu',3}c_{\mathbf{n}+(1,-1),\mu',B}] + \text{H.c.}, \quad \text{(C11)}$$

where $c_{\mathbf{n},\mu,s}$ are electron annihilation operators and $t_{\mu,\mu',j}$ for $j=1,2,3$ are the hopping integrals between orbitals μ and μ' calculated by Eqs. (C7) and (C8) for a bond between a central A atom and its three neighboring B atoms. For a bulk system, this Hamiltonian can be transformed to k-space as usual

$$H_C = \sum_{\mathbf{k}} \left\{ \epsilon_s^C [d^\dagger_{\mathbf{k},0,A} d_{\mathbf{k},0,A} + d^\dagger_{\mathbf{k},0,B} d_{\mathbf{k},0,B}] + \left[\sum_{\mu,\mu'} d^\dagger_{\mathbf{k},\mu,A} f_{\mu\mu'}(\mathbf{k}) d_{\mathbf{k},\mu',B} + \text{H.c.} \right] \right\}, \quad \text{(C12)}$$

where

$$f_{\mu\mu'}(\mathbf{k}) = t_{\mu,\mu',1} + t_{\mu,\mu',2}e^{-ik_2} + t_{\mu,\mu',3}e^{i(k_1-k_2)}, \quad \text{(C13)}$$

and

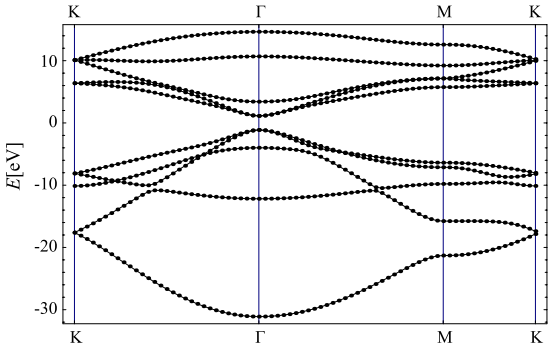

FIG. 7. (Color online) Bulk band structure of graphane calculated from our tight-binding model [Eqs. (C12) and (C15)].

$$d_{\mathbf{k},\mu,s} = \frac{1}{\sqrt{N}} \sum_{n_1,n_2} e^{-i(k_1 n_1 + k_2 n_2)} c_{\mathbf{n},\mu,s}. \quad \text{(C14)}$$

Note that k_1, k_2 are the components of the k-space coordinate with respect to the reciprocal vectors, which are nonorthogonal. In terms of k_x and k_y we have $k_1=\sqrt{3}k_x$ and $k_2=\frac{1}{2}(\sqrt{3}k_x+3k_y)$.

The graphene regions of the heterostructures are fully described by H_C. In the graphane region, the hydrogen-related terms must be added to H_C. Because we only consider nearest-neighbor hopping and the chair conformation of graphane, direct interhydrogen hopping is not allowed. Since the hydrogen atoms are supposed to sit nicely on top ($z>0$) of the B sites and below the A sites ($z<0$), the only non-zero hopping integrals, allowed by symmetry, are the two between the hydrogen $1s$-orbital and the carbon $2s$- and $2p_z$-orbitals, i.e., W_{ss} and W_{sp}, respectively. Because of this perfect alignment, no further transformation of the hopping integrals is needed. Only, because the $2p_z$-orbital points in positive z-direction at the A- as well as at the B-sites, we have to respect the different sign of the sp-hopping between the carbon atoms on A-sites and their attached hydrogen atoms and those on B-sites. We find

$$H_{H-C} = \sum_{\mathbf{k},s} \{\epsilon_s^C d^\dagger_{\mathbf{k},H,s} d_{\mathbf{k},H,s} + [W_{ss} d^\dagger_{\mathbf{k},H,s} d_{\mathbf{k},0,s} + (-1)^s W_{sp} d^\dagger_{\mathbf{k},H,s} d_{\mathbf{k},3,s} + \text{H.c.}]\}. \quad \text{(C15)}$$

The spinless bulk Hamiltonian $H=H_C+H_{H-C}$ can be represented as a $\mathbf{k}$-dependent (10×10)-dimensional matrix, which is easily diagonalized. Figure 7 shows the graphane band structure calculated from H. Compared to the first-principles band structure of Sofo *et al.*,[11] the band width of the lowest band is somewhat larger in our tight-binding model. This is typical for tight-binding models on honeycomb lattices with only nearest-neighbor hoppings and orthogonal orbital wave functions. The band gap is with $E_g \simeq 2.4$ eV smaller than the one found in Refs. 11 and 29. However, since our qualitative considerations are not sensitive to the graphane band gap and since there is neither theoretical consensus nor experimental verification of the size of the band gap, yet, we have chosen to ignore this deficiency here. Note that the band gap can be tuned to higher values by changing the hopping parameters within their fluc-

tuation found from the literature. We have checked that our results are stable with respect to such parameter changes.

For modeling graphane-terminated graphene nanoribbons which are lattice-translationally invariant along the $\mathbf{a}_1$-direction (zigzag ribbons), we perform a partial Fourier transform of the carbon-electron operators, i.e.,

$$d_{n,k,\mu,s} = \frac{1}{N_x}\sum_{n'} e^{-ikn'} c_{n',n,\mu,s}. \tag{C16}$$

The ribbon Hamiltonian in the carbon subspace then reads

$$H_C = \sum_{k,n,\mu,\mu'} d^{\dagger}_{n,k,\mu,A}[t_{\mu,\mu',1} d_{n,k,\mu',B} + (t_{\mu,\mu',2} + e^{ik} t_{\mu,\mu',3}) d_{n-1,k,\mu',B}] + \text{H.c.} \tag{C17}$$

It is important to note that the hopping integrals $t_{\mu,\mu',j}$ are different in the graphane and graphene regions. At the interfaces we assume that the carbon atoms in the last graphane row have the sp^3-like orbital configuration of graphane rather than the sp^2 configuration of graphane. There is some ambiguity in this choice. Different choices of the interface properties do not lead to qualitatively different results. Only the magnitude of the interface-induced spin-orbit splitting and the details of the edge state dispersion may be renormalized by factors of order one.

The hydrogen part of the Hamiltonian is easily added to the graphane regions, as explained above.

APPENDIX D: SPIN-ORBIT HAMILTONIAN

We restrict ourselves to the on-site spin-orbit interaction generated by the Hamiltonian

$$H_{SO} = \underbrace{\frac{\hbar}{4m^2c^2}}_{\equiv A}(\nabla V(\mathbf{r}) \times \hat{\mathbf{p}}) \cdot \boldsymbol{\sigma}, \tag{D1}$$

where $V(\mathbf{r})$ is the (*a priori* unknown) potential of the carbon ions, $\hat{\mathbf{p}} = -i\hbar(\partial_x, \partial_y, \partial_z)$ is the momentum operator of an electron, and $\boldsymbol{\sigma} = (\sigma^x, \sigma^y, \sigma^z)$ are the Pauli matrices for the electron spin. We are interested in the matrix elements of H_{SO} in the subspace spanned by the carbon $2s$- and $2p$-orbitals, i.e., the states $|\psi_{\mu,\tau}\rangle \equiv |\mu,\tau\rangle \equiv |\mu\rangle \otimes |\tau\rangle$ where $\mu = 0,1,2,3$ labels the s-, p_x-, p_y-, p_z-orbital, respectively, and $\tau = \uparrow, \downarrow$ labels the spin.

$$\langle \mu,\tau|H_{SO}|\mu',\tau'\rangle = A\sum_{i=x,y,z} \langle \mu|[\nabla V(\mathbf{r}) \times \hat{\mathbf{p}}]_i|\mu'\rangle \sigma^i_{\tau\tau'}. \tag{D2}$$

Now we perform an explicit calculation of the matrix elements and relate all non-zero integrals to each other by symmetry considerations. In real space, we can write $(i,j,k = x,y,z)$

$$\langle \mu|[\nabla V(\mathbf{r}) \times \hat{\mathbf{p}}]_i|\mu'\rangle = -i\epsilon^{ijk}\int d^3\mathbf{r}\, \psi^*_{\mu}(\mathbf{r})(\partial_j V)\partial_k \psi_{\mu'}(\mathbf{r}), \tag{D3}$$

where we used the wave functions defined in Eq. (C5). From the symmetry of the orbital wave functions and the potential $V(\mathbf{r})$ it is easy to see that

$$\langle s|H_{SO}|p_i\rangle = \langle p_i|H_{SO}|s\rangle = 0, \tag{D4}$$

$$A\langle p_i|[\nabla V \times \hat{\mathbf{p}}]_j|p_k\rangle = i\epsilon^{ijk}\Delta, \tag{D5}$$

where ϵ^{ijk} is the Levi-Civita tensor and

$$\Delta = \frac{\hbar}{4m^2c^2}\int_0^{\infty} dr r|f_p(r)|^2 V'(r). \tag{D6}$$

In second quantization the Hamiltonian reads

$$H_{SO} = i\Delta\sum_{\mathbf{n},s}\sum_{\substack{\mu,\nu,\eta \\ \tau\tau'}} \epsilon^{\mu\nu\eta} c^{\dagger}_{\mathbf{n},\mu,s,\tau}\sigma^{\nu}_{\tau\tau'} c_{\mathbf{n},\eta,s,\tau'}, \tag{D7}$$

where $\mu,\nu,\eta = x,y,z$. The coupling constant $\Delta \simeq 3$ meV is determined from the atomic spin-orbit interaction (see, e.g., Ref. 7).

APPENDIX E: GRAPHANE-TERMINATED $\alpha\beta$-RIBBONS

As mentioned above, there is some ambiguity in the alignment of the interface bonds. There are two extreme cases. The first is shown in Fig. 1: there, the interface bonds are completely in-plane, as if they would correspond to the graphene region. The other extreme case would be that the bonds between the graphene and the graphane region are aligned as if the first graphene atom was sp^3-hybridized, i.e., they are tilted out of the xy-plane just as all other bonds in the graphane region. It is not known to which extent the bonds are tilted out of the plane. This detail is, however, not important for our qualitative considerations.

In the following we quantify the tilting at the interface by a parameter z_J. The fully tilted situation is described by setting $z_J = z_0$. The flat interface (as shown in Fig. 1), on the other hand, is described by $z_J = 0$.

The impact of the interface details on the dispersion of the GG interface state is shown in Fig. 8. Obviously, primarily the edge states are affected by the interface details while the bulk dispersion is largely invariant. Also it is observed that, while the α-edge state's dispersion always resembles a parabola very closely, the β-edge state changes the shape of its dispersion more heavily. However, for this work only the dispersion near K and K' is important. There, changing z_J mainly renormalizes the interface state velocity by a factor of order unity.

In the numerical diagonalization of the $\alpha\beta$-ribbon Hamiltonian the dispersion of the β-edge states are sometimes (depending on the interface details) crossed by bands which are exponentially localized at the outer graphane edge (see Fig. 8). Usually, this crossing happens at $|k| \lesssim 0.2\pi$. These states are spatially separated from the edge states at the interfaces

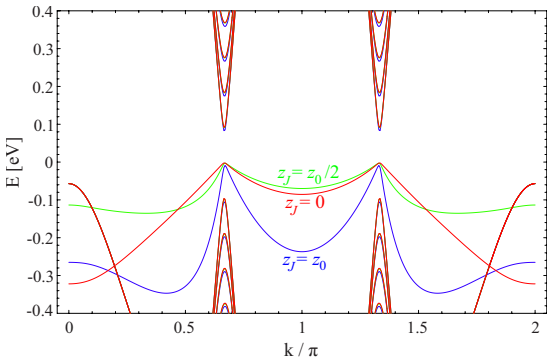

FIG. 8. (Color online) Different band structures for $z_J=0$ (red), $z_J=z_0/2$ (green) and $z_J=z_0$ (blue). The graphene part of the $\alpha\beta$-ribbon is 21 nm wide in this calculation and the graphane terminations are 2.1 nm wide. The bulk states and the states at the outer graphane edges are not significantly affected by z_J. The corresponding energy bands lie on top of each other for the three cases.

and are thus not important here. If the graphane regions were infinitely wide, these bands would not affect the β-edge state at all. However, since the numerical calculations use a finite size ribbon, these graphane edge states have an exponentially small overlap with the β-edge state wave function. Since we are generally interested in the band structure near K and K', this crossing is not important for our reasoning. Thus, in the plots of the numerical spin-splitting and the spin-orbit strength (see below), we leave out the part of the Brillouin zone which is beyond the crossing. This is why the plots of some numerical results are restricted to the k-range $[0.2\pi, 1.8\pi]$.

APPENDIX F: EFFECTIVE SPIN-ORBIT HAMILTONIAN

The effective spin-orbit Hamiltonian of the edge states at the GG interface is obtained by projecting H_{SO} [see Eq. (D7)] to the restricted Hilbert space of the edge states $|\psi^\alpha(k);\tau\rangle$. This leads to an effective SOI described by

$$\Gamma_{\tau\tau'}(k) = \langle \psi^\alpha(k);\tau | H_{SO} | \psi^\alpha(k);\tau' \rangle, \tag{F1}$$

which can be decomposed by means of spin Pauli matrices. It turns out that the function which multiplies σ^x is zero while the coefficient functions of $\sigma^{y/z}$ are finite. This makes sense because in addition to the intrinsic SOI of pure graphene, there is a $z\to -z$ symmetry breaking at the interface which leads to a Rashba-like term $k_x\sigma^y$. The $x\to -x$ symmetry, however, is not broken by the interface so that the Dresselhaus-like term $k_x\sigma^x$ vanishes.

The function $\Gamma_{\tau\tau'}(k)$ can be calculated numerically from the wave functions of the GG edge states. However, it can also be well approximated by an analytic form, constructed from the following reasoning: the spin-orbit interaction at the GG interface is strong compared to the spin-orbit interaction in bulk graphene. Therefore, an effective model must respect the renormalization of the SOI by the amplitude of the interface state wave function directly at the interface. This is given by $\mathcal{N}_k^\alpha$ ($\mathcal{N}_k^\beta$) for α- (β-) edge states in infinitely wide ribbons. Moreover, because of time-reversal invariance, the

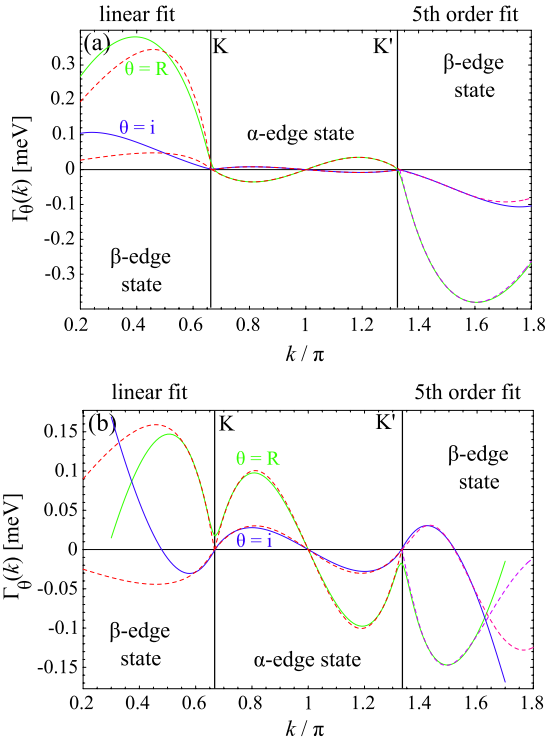

FIG. 9. (Color online) Spin-orbit strength $\Gamma_\theta(k)$, $\theta=i,R$ from the effective model (dashed lines) and from our extended tight-binding model (solid lines). The gray (green) line represents the Rashba term of the spin-orbit Hamiltonian and the nearby dashed lines represent the corresponding terms from the effective models. The black (blue) line represents the intrinsic term of the spin-orbit Hamiltonian. The effective Hamiltonian of the α-edge state is Eq. (F2). The effective Hamiltonian of the β-edge state on the left-hand side (the region labeled by linear fit) is given by the linear version Eq. (F3) while on the right-hand side (the region labeled by 5th order fit), Eq. (F4) is shown. Part (a) shows a calculation for a flat interface ($z_J=0$) and part (b) shows a calculation for a maximally tilted interface ($z_J=z_0$).

k-dependent coupling strength must be odd at $k=0,\pi$. Thus, we only take into account odd polynomials around these two points.

As it turns out, the linear terms are sufficient to fit the numerics of the α-edge state. For the β-edge state more terms are needed for a quantitative fit. This is in part due to the graphane bulk bands which come close to the β-edge states in energy. We checked that the linear fit for $\Gamma^{\text{eff}}_{SO,\beta}(k)$ becomes better if we artificially increase the graphane band gap by tuning the tight-binding parameters.

The form of the effective spin-orbit interaction of the α- and β-edge states with only linear terms reads

$$\Gamma^{\text{eff}}_{SO,\alpha}(k) = (k-\pi)(\mathcal{N}_k^\alpha)^2[\Delta_R^\alpha\sigma^y + \Delta_i^\alpha\sigma^z], \tag{F2}$$

$$\Gamma^{\text{eff}}_{SO,\beta}(k) = k(\mathcal{N}_k^\beta)^2[\Delta_R^\beta\sigma^y + \Delta_i^\beta\sigma^z]. \tag{F3}$$

In order to find the parameters $\Delta_R^{\alpha/\beta}$ and $\Delta_i^{\alpha/\beta}$, we fit these functional forms to the numerical results. Figure 9 shows various fits. In Table II, the effective spin-orbit parameters for the flat ($z_J=0$) and the tilted ($z_J=z_0$) interfaces are given.

TABLE II. Single parameter fit of the spin-orbit interaction for the edge states at α- and β-interfaces.

	$z_j=0$ (meV)	$z_J=z_0$ (meV)
Δ_R^α	−0.090	−0.26
Δ_i^α	0.021	−0.077
Δ_R^β	0.43	0.20
Δ_i^β	0.060	−0.055

The α-edge state spin-orbit interaction is well reproduced by the effective form given in Eq. (F2) while the β-edge state spin-orbit interaction is not. Therefore, we include higher powers in Eq. (F3)

$$\Gamma_{SO,\beta}^{\text{eff}}(k) = k(\mathcal{N}_k^\beta)^2[\Delta_R^\beta(1 + a_R^\beta k^2 + b_R^\beta k^4)\sigma^y + \Delta_i^\beta(1 + a_i^\beta k^2 + b_i^\beta k^4)\sigma^z]. \tag{F4}$$

The parameter fits to the numerical results are given in Table II for the one parameter forms (F2) and (F3) and for the three parameter form (F4) in Table III. In order to compare the effective models with the numerical results, we define the Rashba (intrinsic) spin-orbit strength $\Gamma_R(k)$ [$\Gamma_i(k)$] as the coefficient of the Pauli matrix σ^y (σ^z) in the expressions (F1)–(F4). Figure 9 compares the different expressions. Obviously, the linear expression (F2) is sufficient for the α-edge state while (F3) shows significant deviations from the numerical results for the β-edge state.

The spin-splitting $\Delta\epsilon_{SO}(k)$ calculated from the effective model is in better agreement with the numerical results than the spin-orbit strengths $\Gamma_\theta(k)$ (see Fig. 3), even for the linear model of the β-edge state, because this quantity is an average over the intrinsic and Rashba term of the spin-orbit Hamiltonian.

For infinitely wide ribbons ($W\to\infty$), the normalization factors $\mathcal{N}_k^{\alpha/\beta}$ vanish at K,K'. Thus, the spin-orbit splitting at K,K' is not enhanced by the Hamiltonians (F2)–(F4), compared to pure graphene. In finite size ribbons, however, the normalization of the edge state wave functions is significantly different from $\mathcal{N}_k^{\alpha/\beta}$ if $\xi_k^{\alpha/\beta} > W$. The edge state of a finite size $\alpha\beta$-ribbon with N unit cells in the y-direction can be written as

TABLE III. Three parameter fit of the spin-orbit interaction for the edge state at a β-interface.

	$z_j=0$	$z_J=z_0$
Δ_R^β	0.61 meV	−0.030 meV
a_R^β	−0.13	−4.7
b_R^β	0.006	0.75
Δ_i^β	0.21 meV	0.36 meV
a_i^β	−0.41	−0.65
b_i^β	0.05	0.09

$$|\psi_0(k)\rangle = \sqrt{\frac{1-|u_k|^2}{1-|u_k|^{2(N+1)}}} \times \sum_{n=0}^{N} \exp\left(-\frac{n}{\xi_k^\alpha} + in\phi\right) d_{n,k,B}^\dagger |0\rangle. \tag{F5}$$

At K,K' the absolute value of this wave function is constant in y-direction. Thus, the amplitude at the interface is not proportional to $(\mathcal{N}_K^{\alpha/\beta})^2=0$ in this finite-size case, but rather proportional to

$$\frac{1-|u_k|^2}{1-|u_k|^{2(N+1)}} \xrightarrow{k\to K,K'} \frac{1}{N_y+1}. \tag{F6}$$

As a result, the GG interface-induced SOI near K,K' is proportional to W^{-1}. Thus, the SOI of bulk graphene becomes dominant at K,K' in the limit $W\to\infty$.

This is important for the QSVHE in that the Fermi energy must be tuned exactly to the spin-orbit gap which is due to the bulk graphene SOI. Qualitatively, this bulk SOI can be included in the effective model by adding the bulk graphene-induced spin-orbit splitting of the edge states at K,K',[30]

$$H_{SO,\alpha/\beta}^{\text{eff}} \to H_{SO,\alpha/\beta}^{\text{eff}} + \Delta_0\sigma^z\tau^3, \tag{F7}$$

where $2\Delta_0 \sim \mu$eV is the spin-orbit gap at K,K' in bulk graphene and $\tau^3=\pm 1$ for K and K', respectively.

[1] K. v. Klitzing, G. Dorda, and M. Pepper, Phys. Rev. Lett. **45**, 494 (1980).
[2] C. L. Kane and E. J. Mele, Phys. Rev. Lett. **95**, 226801 (2005).
[3] M. König, S. Wiedmann, C. Brune, A. Roth, H. Buhmann, L. W. Molenkamp, X.-L. Qi, and S.-C. Zhang, Science **318**, 766 (2007).
[4] X.-L. Qi, T. L. Hughes, and S.-C. Zhang, Phys. Rev. B **78**, 195424 (2008).
[5] K. S. Novoselov, A. K. Geim, S. V. Morozov, D. Jiang, S. V. Dubonos, I. V. Grigorieva, and A. A. Firsov, Science **306**, 666 (2004).
[6] A. H. Castro Neto, F. Guinea, N. M. R. Peres, K. S. Novoselov, and A. K. Geim, Rev. Mod. Phys. **81**, 109 (2009).
[7] H. Min, J. E. Hill, N. A. Sinitsyn, B. R. Sahu, L. Kleinman, and A. H. MacDonald, Phys. Rev. B **74**, 165310 (2006).
[8] X. Jia, M. Hofman, V. Meunier, B. G. Sumpter, J. Campos-Delgado, J. M. Romo-Herrera, H. Son, Y.-P. Hsieh, A. Reina, J. Kong, M. Terrones, and M. S. Dresselhaus, Science **323**, 1701 (2009).
[9] K. S. Novoselov, Phys. World **22**, 27 (2009).
[10] A. K. Singh and B. I. Yakobson, Nano Lett. **9**, 1540 (2009).
[11] J. O. Sofo, A. S. Chaudhari, and G. D. Barber, Phys. Rev. B **75**, 153401 (2007).
[12] D. C. Elias, R. R. Nair, T. M. G. Mohiuddin, S. V. Morozov, P. Blake, M. P. Halsall, A. C. Ferrari, D. W. Boukhalov, M. I. Katsnelson, A. K. Geim, and K. S. Novoselov, Science **323**, 610 (2009).
[13] P. Koskinen, S. Malola, and H. Häkkinen, Phys. Rev. B **80**,

073401 (2009).
[14] Though, single dangling bonds have been observed experimentally (see Ref. 31).
[15] M. Kohmoto and Y. Hasegawa, Phys. Rev. B **76**, 205402 (2007).
[16] Ken-ichi Sasaki, Kentaro Sato, Riichiro Saito, Jie Jiang, Seiichiro Onari, and Yukio Tanaka, Phys. Rev. B **75**, 235430 (2007).
[17] W. Yao, S. A. Yang, and Q. Niu, Phys. Rev. Lett. **102**, 096801 (2009).
[18] M. Fujita, K. Wakabayashi, K. Nakada, and K. Kusakabe, J. Phys. Soc. Jpn. **65**, 1920 (1996).
[19] Y.-W. Son, M. L. Cohen, and S. G. Louie, Nature (London) **444**, 347 (2006).
[20] E. H. Lieb, Phys. Rev. Lett. **62**, 1201 (1989).
[21] M. J. Schmidt and D. Loss (unpublished).
[22] For the QVHE in graphene bilayers and due to the superconducting proximity effect see Refs. 32 and 33, respectively.
[23] B. C. Pan, Phys. Rev. B **64**, 155408 (2001).
[24] M. S. Tang, C. Z. Wang, C. T. Chan, and K. M. Ho, Phys. Rev. B **53**, 979 (1996).
[25] V. Tozzini and V. Pellegrini, Phys. Rev. B **81**, 113404 (2010).
[26] L. Openov and A. Podlivaev, JETP Lett. **90**, 459 (2009).
[27] R. Saito, G. Dresselhaus, and M. S. Dresselhaus, *Physical Properties of Carbon Nanotubes* (Imperial College Press, London, 1999).
[28] S. Reich, J. Maultzsch, C. Thomsen, and P. Ordejon, Phys. Rev. B **66**, 035412 (2002).
[29] S. Lebegue, M. Klintenberg, O. Eriksson, and M. I. Katsnelson, Phys. Rev. B **79**, 245117 (2009).
[30] The bulk graphene-induced spin-orbit splitting of the edge states is k dependent. However, it is sufficient to take only the value of the splitting at K, K'.
[31] Z. Liu, K. Suenaga, P. J. F. Harris, and S. Iijima, Phys. Rev. Lett. **102**, 015501 (2009).
[32] I. Martin, Y. M. Blanter, and A. F. Morpurgo, Phys. Rev. Lett. **100**, 036804 (2008).
[33] P. Ghaemi, S. Ryu, and D. Lee, Phys. Rev. B **81**, 081403(R) (2010).